Mode Recovery by S^2 Imaging Without a Fourier Transform

Yves Quiquempois, Benoit Sevigny, Esben Ravn Andresen, Alex Chedid, Laurent Bigot

Mode Recovery by S^2 Imaging Without a Fourier Transform

Yves Quiquempois , Benoit Sévigny , Esben Ravn Andresen, Alex Chedid , and Laurent Bigot

***Abstract*—In its standard implementation, spatially and spectrally resolved (S^2) imaging consists in recording near field intensity patterns as a function of the wavelength, followed by a Discrete Fourier Transform (DFT) to assess differential group delays, as well as optical power distribution between modes for the given injection as long as the higher-order mode powers are low. Here we present a variant of S^2-imaging which does not make use of DFT. The method is more robust to wavelength jitter of the laser source. Furthermore, in special cases, the method allows retrieving relative modal powers without constraints on HOM power.**

***Index Terms*—Optical fiber, guided modes, mode content.**

I. Introduction

SPATIALLY and spectrally resolved (S^2) imaging is a powerful technique for characterizing mode content in an optical fiber. Indeed, with a very simple experimental setup (a camera, a tunable laser, and basic optical components) [1], beating between modes resulting from the difference in their group delays as they propagate through the fiber, can be recorded at its output end as a function of the wavelength, λ. In many cases, a simple DFT allows beating between only two modes (the fundamental one – in general – and a Higher-Order Mode (HOM)) to be isolated [2], leading to the determination of their group delay difference, and their power distribution. This method, which we will refer to as "standard S^2 imaging," has been first developed by J. W. Nicholson *et al.* [2], [3], and is now a common tool for assessing the mode content of fibers used, for example, in the field of fiber lasers where the presence of HOMs is detrimental to beam quality [4], or in the field of multimode telecommunications where several modes can be used to carry information [5].

This work was supported in part by the French Agence Nationale de la Recherche: Equipex Flux (ANR-11-EQPX-0017), Labex CEMPI (ANR-11-LABX-0007), and ANR MUPHTA (ANR-20-CE24-0016); the Ministry of Higher Education and Research; the Hauts-de-France Regional Council and in part by the European Regional Development Fund (ERDF) through the Contrat de Plan Etat-Region (C.P.E.R. Photonics for Society, P4S).

Yves Quiquempois, Esben Ravn Andresen, Alex Chedid, and Laurent Bigot are with the Univ. Lille, CNRS, UMR 8523 – PhLAM – Physique des Lasers, Atomes et Molécules, F-59000 Lille, France (e-mail: yves.quiquempois@univ-lille.fr; esben.andresen@univ-lille.fr; alex.chedid@univ-lille.fr; laurent.bigot@univ-lille.fr).

Benoit Sévigny is with ITF Technologies, 400 Montpellier Blvd, Saint-Laurent, Quebec H4N 2G7, Canada (e-mail: bsevigny@protonmail.com).

In 2014, our group developed an advanced S^2 (A-S^2) imaging method to recover the modal content in few-mode fibers [6]. The difference as compared to the standard S^2 imaging lies in a specific data processing of the recorded images. Instead of analyzing the data directly in the Fourier domain, spatial correlations are first analyzed between images obtained at different wavelengths; Principal Component Analysis (PCA) and Independent Component Analysis (ICA) are thus applied to the data set. A-S^2 allows some mixed beatings that cannot be recovered otherwise to be extracted from the mixed signals. PCA and ICA are well-known statistical methods used in the domain of deep-learning and multivariate analysis for blind source reconstruction.

To measure the differential group delays between modes, a trade-off has to be found (as in the standard S^2 method) between the length L of the Fiber Under Test (FUT), the tuning step in wavelength ($\delta\lambda$), and the total wavelength span of the laser source. This limitation comes naturally from the sampling rate of the DFT and the Nyquist criterion. Assuming that the central wavelength is λ_0 and that the total wavelength range over which images are recorded is $\Delta\lambda = \mathcal{N}\delta\lambda$, $\mathcal{N}$ being the number of samples, the relative group index difference Δn_g that can be measured is approximately in the range:

$$\frac{1}{L}\frac{\lambda_0^2}{\mathcal{N}\delta\lambda} \leq \Delta n_g \leq \frac{1}{2L}\frac{\lambda_0^2}{\delta\lambda} \tag{1}$$

Moreover, from a practical point of view, the tuning step $\delta\lambda$ should be accurate enough (i.e. constant) as λ varies otherwise peaks in the Fourier domain may be completely washed out, meaning that, depending on the laser type, a wavelength meter should be used in parallel.

In this present paper, we show that the sole analysis of correlations between images recorded at different wavelengths can be sufficient to identify the modal content without performing a DFT, meaning that a constant wavelength step size is not mandatory in this case. If we assume that one mode is dominant (in terms of optical power), or if beatings between excited modes are mutually orthogonal, Multi-Path Interferences (MPI) can be obtained.

The paper will be organized as follows: in Section II, basic equations describing the evolution of beatings in the fiber will be recalled. Section III will be devoted to the description of matrix notation and analysis of beating orthogonality. Section IV corresponds to the mathematical development at the heart of our approach: it shows how beatings and modal powers can be extracted for different configurations. In Section V, a study of

TABLE I
BEATING NOTATION

Reduced variable	Expression
$M = N(N-1)/2$	Total number of beatings
i	kl
$B_i(x,y)$	$F_k(x,y)F_l(x,y)$
Π_i	$2\sqrt{P_k P_l}$
$\hat{e}_i$	$\cos(\omega\tau_{kl} + \phi_{kl})$

wavelength jitter will be presented through a numerical example, and finally some conclusions will be drawn.

II. Basic Equations Governing Modal Interference in a Multimode Fiber

The electric field associated to guided mode k of a fiber that is translationally invariant can be expressed as follows (assuming linearly polarized fields):

$$E_k(x,y,z,\omega) = \sqrt{P_k}F_k(x,y)e^{i\omega t}e^{-i\beta_k z} \tag{2}$$

where F_k is the mode envelope, β_k the propagation constant, ω the angular frequency and $\sqrt{P_k}$ the amplitude of the corresponding electric field.

Scalar product in space can be defined by :

$$\langle F_i|F_j\rangle = \int_{A_\infty} F_i F_j \mathrm{d}A = A_i\delta_{ij} \tag{3}$$

where A_i is the normalization constant for field i, A_∞ is the area of the cross-section and δ_{ij} is the Kronecker delta.

Assuming N guided modes, the near field intensity I recorded after a length L of the FUT can be expressed as [6]:

$$I = \overline{I} + \sum_{k=1}^{N-1}\sum_{l=k+1}^{N} 2\sqrt{P_k P_l}F_k F_l \cos(\tau_{kl}\omega + \phi_{kl}) \tag{4}$$

where τ_{kl} is the relative time delay between mode k and mode l, and ϕ_{kl} is a phase constant. $\overline{I}$ is the constant part of the intensity (mean value over λ).

τ_{kl} is related to the fiber length L and the group index difference Δn_g by:

$$\tau_{kl} = \frac{L}{c}\Delta n_{g,kl} \tag{5}$$

c being the speed of light in vacuum.

After removing the constant component $\overline{I}$ from the total intensity, Eq. (4) can be re-written by using the beating notation described in Tab. (I).

$$\tilde{I} = I - \overline{I} = \sum_{i=1}^{M} \Pi_i B_i \hat{e}_i \tag{6}$$

Eq. (6) is the starting point of the A-S^2 analysis.

We will use hereafter the bra-ket notation for transverse fields and beatings: $|B_i\rangle = |F_k F_l\rangle$. Π_i will be called "beating power" to avoid confusion with power P_k carried by guided mode k.

Two remarks can be made at this point in light of this theoretical framework: (i) we can define a scalar product in the wavelength domain for the cosines:

$$(\hat{e}_i, \hat{e}_j) = \frac{1}{\Delta\omega}\int_{\Delta\omega} \hat{e}_i\hat{e}_j \mathrm{d}\omega \tag{7}$$

meaning that $2(\hat{e}_i, \hat{e}_j) = \delta_{ij}$ if $\Delta\omega$ (which corresponds to the total range in wavelengths in the experiment) is sufficiently large and if we assume that each relative time delays τ_i are different, and (ii) while field envelopes are orthogonal to each other, i.e. $\langle F_i|F_j\rangle = 0$, $\forall i \neq j$, figures of beatings are not in general: $\langle B_i|B_j\rangle \neq 0$ for some $i \neq j$.

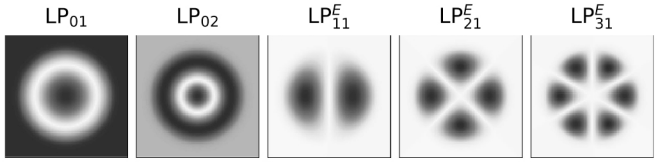

(a) Example of excited modes in a multimode step-index fiber

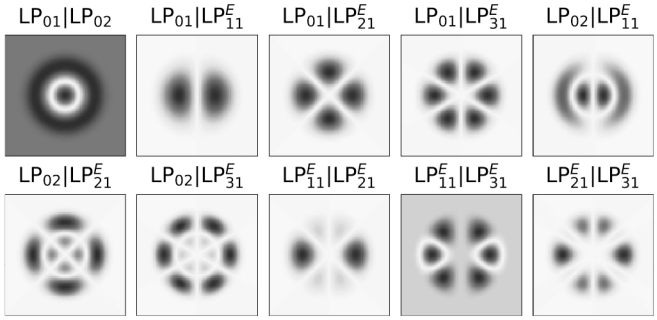

(b) Resulting beating figures

Fig. 1. Ten beating patterns of a low contrast step-index multimode fiber having 5 excited modes LP $_{01}$, LP$^E_{11}$, LP$^E_{21}$, LP$^E_{31}$, and LP$_{02}$. First row: beatings $|B_1\rangle$ to $|B_5\rangle$, second row, beatings $|B_6\rangle$ to $|B_{10}\rangle$. For example, $|B_5\rangle$ is LP$_{02}$|LP$^E_{11}$.

In the following, we will demonstrate our results using, as an example, an ideal step-index fiber having a refractive index contrast Δn of $30{\cdot}10^{-3}$ and a core radius of 10 μm. The refractive index is assumed to be non-dispersive. Fig. 1(a) shows examples of excited modes, together with resulting beating patterns (Fig. 1(b)). Only even modes (superscript E) are used in this example since odd modes show the same group index in the weak guidance approximation.

Numerical results have been obtained using a home-made scalar mode solver based on higher-order finite elements method.

As per [2], we define the Multi-Path Interference MPI of mode k as being:

$$\mathrm{MPI}_k = 10\log\frac{P_k}{P_{\mathrm{major}}} \quad [\mathrm{dB}] \tag{8}$$

P_{major} corresponds to the dominant mode guided in the fiber with highest power (usually the fundamental mode LP$_{01}$).

III. Matrix Notation

We will assume in the following that beating patterns will not change significantly as a function of wavelength. This assumption is not a strong condition since generally the wavelength scanning range for an S^2 method is small (typically 1–2 nm depending on the fiber length L used). Images contain a number of pixels P. Pixels basis $|p\rangle$ is orthonormal meaning that $\langle p|p'\rangle = \delta_{pp'}$.

Each beating $|B_i\rangle$ is decomposed onto the pixel basis $|p\rangle$ through:

$$|B_i\rangle = \sum_{p=1}^{P} b_{pi} \, |p\rangle \tag{9}$$

b_{pi} representing the intensity recorded on pixel p.

Matrix $\mathbf{B}$ (dimension $P \times M$) is defined as being the matrix of beatings where each column corresponds to $|B_i\rangle$, $i \in \{1, \ldots, M\}$ in pixel basis:

$$\mathbf{B} = \left(|B_1\rangle, |B_2\rangle, \ldots, |B_i\rangle, \ldots, |B_M\rangle\right) \tag{10}$$

We define also matrix $\hat{\mathbf{P}}$ (dimension $M \times M$) where element on row i and column j is equal to $\Pi_i \Pi_j (\hat{e}_i | \hat{e}_j)$. According to Eq. (7), we can assume that this matrix is diagonal:

$$\hat{\mathbf{P}} = \frac{1}{2} \begin{pmatrix} \Pi_1^2 & 0 & \cdots & 0 \\ 0 & \Pi_2^2 & \cdots & 0 \\ \vdots & & \ddots & 0 \\ 0 & 0 & \cdots & \Pi_M^2 \end{pmatrix} \tag{11}$$

Similarly, intensity patterns recorded for each λ_i can be shaped into a matrix called $\mathbf{X}$ (dimension $P \times \mathcal{N}$), each column being an image taken at wavelength λ_i where the mean intensity value is removed to obtain $\tilde{I}$ (Eq. (6)). $\mathcal{N}$ is the total number of images.

A-S^2 imaging consists first of calculating the variance-covariance matrix $\mathbf{C}$. $\mathbf{C}$ is obtained directly from $\mathbf{X}$ by:

$$\mathbf{C} = \mathcal{N}^{-1} \mathbf{X} \mathbf{X}^T \tag{12}$$

Dividing by $\mathcal{N}$ ensure equality with Eq. (13). After simple linear algebra calculation, and using Eq. (6), we can demonstrate that $\mathbf{C}$ is related to $\mathbf{B}$ and $\hat{\mathbf{P}}$ by:

$$\mathbf{C} = \mathbf{B} \hat{\mathbf{P}} \mathbf{B}^T \tag{13}$$

$\mathbf{C}$ is a real symmetric matrix meaning that it can be diagonalized and eigenvectors are orthogonal to each other. Each eigenvector $|V_i\rangle$ of the variance-covariance matrix $\mathbf{C}$ corresponds to the Principal Components (PCs) of $\mathbf{X}$:

$$\mathbf{C} = \mathbf{V} \mathbf{D} \mathbf{V}^T \tag{14}$$

with $\mathbf{V} = \left(|V_1\rangle, |V_2\rangle, \ldots, |V_P\rangle\right)$ the matrix of eigenvectors, and $\mathbf{D}$ a diagonal matrix.

By definition, $\mathbf{V}$ is an orthonormal matrix, meaning that $\mathbf{V}\mathbf{V}^T = \mathbf{V}^T\mathbf{V} = \mathbf{I}$ where $\mathbf{I}$ is the identity matrix. However, $\mathbf{B}$ is not in general. Indeed Fig. 2 shows a 2D plot of matrix $\mathbf{B}^T\mathbf{B}$ where the element at row i and column j corresponds to the scalar product $\langle B_i | B_j \rangle$. Off-diagonal elements can be observed except for beating $|B_1\rangle$ in this example.

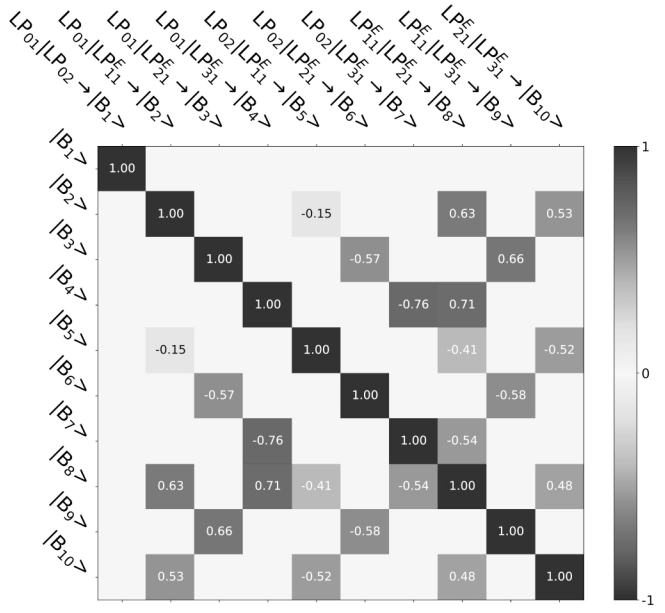

Fig. 2. Matrix showing results of scalar product between beating patterns considered previously. In this figure, beatings have been normalized to unity ($\langle B_i | B_i \rangle = 1$) to reveal noticeable off-diagonal values. Presence of off-diagonal terms means that beatings patterns are not orthogonal to each other. For example, beating $|B_2\rangle$ overlaps with $|B_5\rangle$, $|B_8\rangle$ and $|B_{10}\rangle$.

IV. Analysis of Principal Components and Extraction of Beating Powers Π_i

The purpose of S^2 imaging methods is generally twofold: determine whether HOMs exist in the FUT, and obtain at least beating powers, i.e. $\hat{\mathbf{P}}$, or eventually powers P_i of excited modes.

Diagonal elements in $\mathbf{D}$, and corresponding PCs $|V_i\rangle$ can be obtained easily using standard numerical linear algebra packages knowing experimental matrix $\mathbf{C}$ deduced from Eq. (12). Reconstructing $\hat{\mathbf{P}}$ from $\mathbf{D}$ is however not straightforward. While $\hat{\mathbf{P}}$ and $\mathbf{D}$ are diagonal, they do not share the same dimensions: $P \times P$ for $\mathbf{D}$ and $M \times M$ for $\hat{\mathbf{P}}$.

$\mathbf{B}$ is also different from $\mathbf{V}$ since, (i) they do not have the same dimensions, and (ii) $\mathbf{B}^T\mathbf{B}$ is in general different from $\mathbf{I}$ as shown before. The difficulty presented by point (i) can be overcome by extending matrix $\mathbf{B}$ of dimensions $P \times M$ to $P \times P$ with $P - M$ column vectors constituted by random noise so that its inverse can be calculated. The issue presented in point (ii) however is more problematic, meaning that eigenvectors $|V_i\rangle$ obtained by diagonalizing $\mathbf{C}$ are not stricto sensu figures of beating $|B_i\rangle$.

We will discuss in the next sections how to reconstruct beating figures and beating powers in some particular cases.

A. General Case - No Constraint on MPI

With the knowledge of $\mathbf{D}$ and $\mathbf{V}$ from $\mathbf{X}$, matrix $\hat{\mathbf{P}}$ can be reconstructed using Eq. (15) below:

$$\hat{\mathbf{P}} = \tilde{\mathbf{B}}^{-1} \mathbf{C} (\tilde{\mathbf{B}}^T)^{-1} = \tilde{\mathbf{B}}^{-1} \mathbf{V} \mathbf{D} \mathbf{V}^T (\tilde{\mathbf{B}}^T)^{-1} \tag{15}$$

where $\tilde{\mathbf{B}}$ corresponds to matrix $\mathbf{B}$ extended with extra columns made of random noise as written above.

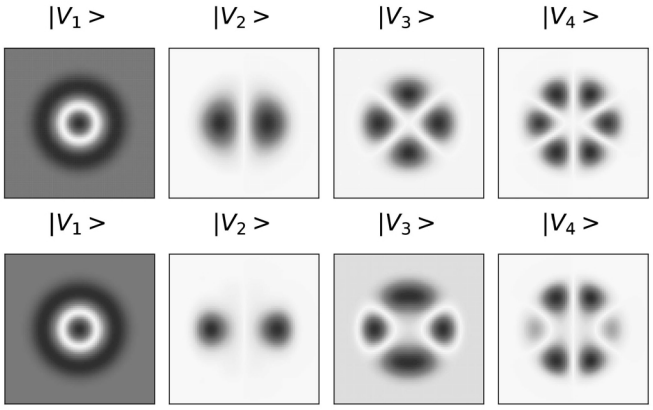

Fig. 3. Example of PC patterns obtained by diagonalizing $\mathbf{C}$. **Top Row**: First four eigenvectors when MPI values for HOMs is -30 dB. **Bottom Row**: PCs for HOM having MPI of - 3 dB. While at low powers $|V_i\rangle$ correspond to beatings, at higher powers, PCs are clearly deformed except for $|V_1\rangle$.

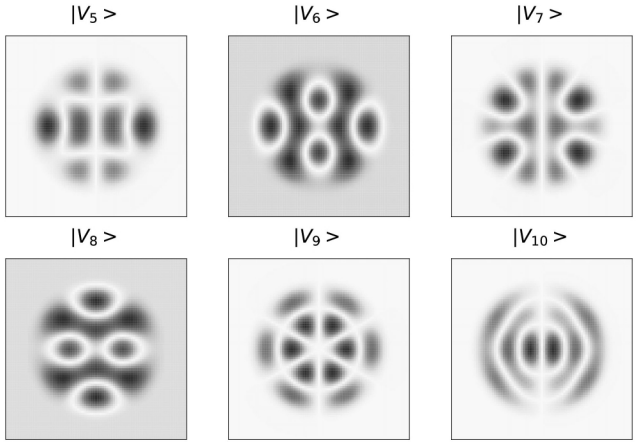

Fig. 4. Last six eigenvectors for an MPI of -30 dB. One can observe that these eigenvectors differ completely from beating patterns except for $|V_9\rangle$ which corresponds to beating $|B_7\rangle$.

This point has been numerically verified in the context of a fiber excited with modes shown in Fig. 1(a) up to a maximal MPI value of -3 dB for HOMs. Exact beating powers Π_i have been correctly obtained.

While very simple at first glance, this general method is in reality not straightforward when dealing with experimental data. Indeed, experimental PCs are not generally oriented along the x- or y-axis of the camera, meaning that the right orientation of guided modes and thus of beatings figures should be determined (it is noticeable here that theoretical guided modes of the FUT can be calculated using the experimental refractive index of the fiber). Nonetheless, this orientation can be directly extracted from the experimental PCs. Most importantly, care should also be taken to sort PCs in the same order than corresponding beating figures which can be tricky if PCs are very different from $|B_i\rangle$, i.e. in the case of high MPI.

B. Case of Low MPI

In the case of low MPI, we will see that simplifications can be made. To start with, let us assume that all guided modes shown in Fig. 1(a), i.e. LP_{01}, LP^E_{11}, LP^E_{21}, LP_{02}, and LP^E_{31}, are excited. We will consider that the fundamental mode LP_{01} is mainly guided with a power normalized to 1.0. Power P of all other above-cited modes is increased from 0.001 to 0.5, meaning that the lowest considered MPI is equal to -30 dB, and the highest is -3 dB.

Matrix $\hat{\mathbf{P}}$ is determined using Eq. (11). Matrix $\mathbf{C}$ is calculated from Eq. (13) to avoid fixing arbitrarily the wavelengths range and the fiber length.

We expect in this example four major beatings (between the fundamental mode and HOMs) with beating powers equal to $\Pi_{\mathrm{major}} = 2\sqrt{P}$, and six minor beatings (between HOMs) carrying beating powers equal to $\Pi_{\mathrm{minor}} = 2P < \Pi_{\mathrm{major}}$.

The first four PCs $|V_i\rangle$ sorted in the same order as beatings figures are displayed in Fig. 3. Top row corresponds to the situation with the lowest and bottom row to the highest MPIs. Comparison of Fig. 1(b) and Fig. 3 shows that beatings patterns and PCs are very similar at low MPI. However, at higher MPI, PCs differ strongly from beatings except for $|V_1\rangle$ which has no overlap with over beatings (see Fig. 2).

Fig. 4 display all the other PCs with smallest eigenvalues in the case of an MPI of -30 dB (sorted by decreasing eigenvalues). Generally, these minor PCs are nearly identical for all values of MPIs explored in this study. As can be seen, these PCs are very different from beating patterns (Fig. 1(b)), except for $|V_9\rangle$ which corresponds to beating $|B_7\rangle$ at this level of power.

To be more quantitative, the PCs $|V_i\rangle$ can be projected onto the beatings as:

$$|V_i\rangle = \sum_{k=1}^{k=M} \alpha_{ki} \, |B_k\rangle \tag{16}$$

The evolution of α_{ii} (corresponding to associated beating $|B_i\rangle$ for low MPI) is reported in Fig. 5 as a function of power in HOMs. To obtain this figure, beatings have been normalized to unity ($\langle B_i|B_i\rangle = 1\,,\ \forall i \in \{1,\ldots,M\}$). As can be seen, the observations made above are confirmed: at low power in higher-order modes, beatings are well approximated by eigenvectors of $\mathbf{C}$ ($\alpha_{ii} \approx 1$), but for higher powers P, PCs become combinations of beatings. For example, projection coefficient α_{22} of $|V_2\rangle$ along beating $|B_2\rangle = \mathrm{LP}_{01}|\ \mathrm{LP}^E_{11}$ is equal to 0.99 for an MPI of -30 dB but decreases monotonously to 0.54 for an MPI of -3 dB, meaning that vector $|V_2\rangle$ is similar to $|B_2\rangle$ by only 54%.

Fig. 6 shows the evolution of $|\alpha_{i2}|$ in the beating figures basis for increasing power in HOMs. For the highest MPI, $|V_2\rangle$ for example is a combination of beatings in the following proportion: $0.54\,|B_2\rangle + 0.15\,|B_4\rangle - 0.08\,|B_5\rangle - 0.06\,|B_7\rangle + 0.29\,|B_8\rangle + 0.22\,|B_{10}\rangle$.

Fig. 7 depicts the evolution of the four first eigenvalues divided by the corresponding quantity $\langle B_i|B_i\rangle$ as a function of power $P_i = P$ in HOM number i (see Eq. (17)). This normalization of eigenvalues is used to compare them directly with diagonal elements of matrix $\hat{\mathbf{P}}$ which should be equal in the case of these major beatings i to $0.5\,\Pi_i^2 = 2P$, meaning that if diagonal elements of $\hat{\mathbf{P}}$ are equal to normalized eigenvalues of $\mathbf{C}$, curves will be superposed to red circles in Fig. 7.

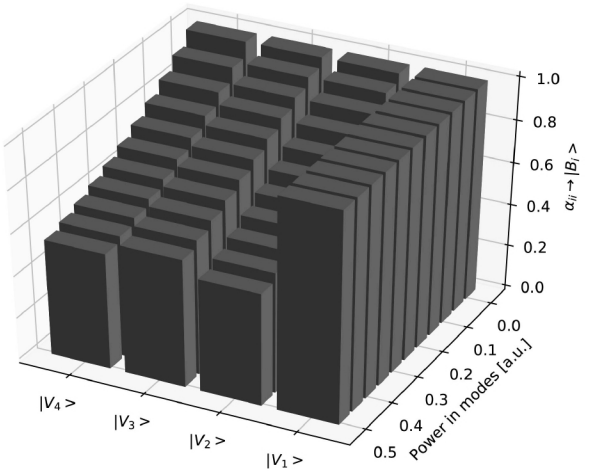

Fig. 5. Percentage of major beating $|B_i\rangle$ found in eigenvector $|V_i\rangle$ as the power in HOMs (LP_{02}, LP_{11}^E, LP_{21}^E, LP_{31}^E) increases from 0.001 to 0.5. Only the 4 first eigenvectors with the highest eigenvalues are shown. Power in mode LP_{01} is set constant to 1. Beating figures have been normalized to 1.0. For example, eigenvector $|V_1\rangle$ is always equal to beating $|B_1\rangle$, but the coordinate of $|V_2\rangle$ onto $|B_2\rangle$ varies from $0.99\,|B_2\rangle$ to $0.54\,|B_2\rangle$ as the power in extra-modes increases, meaning that $|V_2\rangle$ is a mix of some beating figures when the power in each mode becomes important (see Fig. 6).

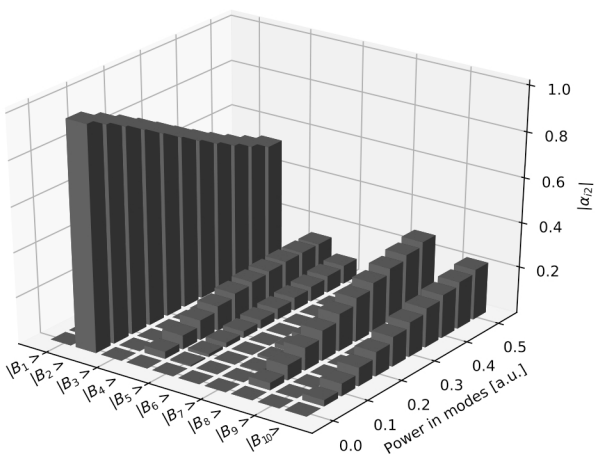

Fig. 6. Evolution of absolute value of coordinates of $|V_2\rangle$ in the basis of beating figures.

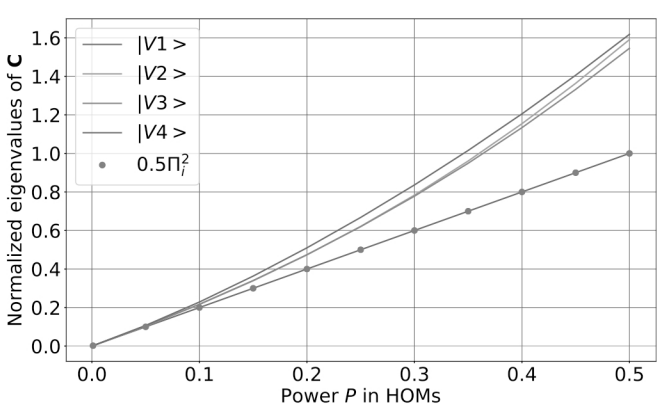

Fig. 7. Major eigenvalues of $\mathbf{C}$ normalized to corresponding $\langle B_i|B_i\rangle$ scalar product as a function of power P in each HOMs (see Eq. (17)). Corresponding diagonal elements of $\hat{\mathbf{P}}$ are displayed with red circles.

The blue curve corresponds to beating $|B_1\rangle = \alpha_{11}\,|V_1\rangle$. Other colors represent the 3 other PC eigenvalues. Two remarks can be drawn here: as expected, for low power in HOMs, normalized eigenvalues are close to diagonal elements of matrix $\hat{\mathbf{P}}$. Moreover, when a beating is orthogonal to the set of all other beatings, its normalized eigenvalue is equal to $0.5\,\Pi_i^2$ which corresponds to the diagonal element of matrix $\hat{\mathbf{P}}$ (see blue curve).

Through this example, we can conclude that major PCs of $\mathbf{X}$ are beating figures $|B\rangle$ in the low-MPI case. Diagonalizing $\mathbf{C}$ allows then to extract major beating figures, and also corresponding beating powers, as diagonal elements of $\mathbf{D}$ are similar to diagonal elements of matrix $\hat{\mathbf{P}}$, provided that eigenvalues are normalized to corresponding scalar products $\langle B_i|B_i\rangle$.

C. Case of a 3-Mode Fiber

In the case of a fiber guiding the fundamental mode LP_{01} and two higher-order modes LP_{11}, and LP_{21}, 3 beatings are expected: $|B_2\rangle$ ($LP_{01}|\,LP_{11}$), $|B_3\rangle$ ($LP_{01}|\,LP_{21}$), and $|B_8\rangle$ ($LP_{11}|\,LP_{21}$) as indexed in Fig. 1. In such a case, only 2 beatings overlap ($|B_2\rangle$ and $|B_8\rangle$). Using Eq. (13) and Eq. (14) together with numerical values of matrix $\mathbf{B}^T\mathbf{B}$ that can be obtained from a mode solver knowing the experimental RIP, one can obtain PCs and corresponding eigenvalues (see Appendix).

If we note σ_2, σ_3, and σ_8 the three eigenvalues associated respectively to $|V_1\rangle = \alpha_{21}\,|B_2\rangle + \alpha_{81}\,|B_8\rangle$, $|V_2\rangle = \alpha_{32}\,|B_3\rangle$, and $|V_3\rangle = \alpha_{23}\,|B_2\rangle + \alpha_{83}\,|B_8\rangle$, simple linear algebra shows that, in the case where the LP_{01} is mainly excited:

$$\begin{cases} \sigma_2 \approx 0.5\,\Pi_2^2\,\langle B_2|B_2\rangle \\ \sigma_3 = 0.5\,\Pi_3^2\,\langle B_3|B_3\rangle \\ \sigma_8 \approx 0.5\,\Pi_8^2\,\langle B_8|B_8\rangle\left(1 - \frac{\langle B_2|B_8\rangle^2}{\langle B_8|B_8\rangle\langle B_2|B_2\rangle}\right) \end{cases} \tag{17}$$

All the coordinates α_{21}, α_{81}, α_{23}, and α_{83} can be also deduced from σ's so that real beatings can be extracted from PCs.

In this simple case, MPI of the two HOMs can be obtained from Eq. (17). The set of equations (18) recall hereafter how to extract ratios of powers:

$$\begin{cases} \frac{P_{11}}{P_{01}} = \frac{\sigma_8}{\sigma_3}\,\frac{\langle B_3|B_3\rangle}{\langle B_8|B_8\rangle\left(1-\frac{\langle B_2|B_8\rangle^2}{\langle B_8|B_8\rangle\langle B_2|B_2\rangle}\right)} \\ \frac{P_{21}}{P_{01}} = \frac{\sigma_8}{\sigma_2}\,\frac{\langle B_2|B_2\rangle}{\langle B_8|B_8\rangle\left(1-\frac{\langle B_2|B_8\rangle^2}{\langle B_8|B_8\rangle\langle B_2|B_2\rangle}\right)} \end{cases} \tag{18}$$

In the case of high MPI, a similar development can be obtained from equations shown in the Appendix. Note that the case of 3-mode fiber can be also extended to a fiber supporting more guided modes but has not been developed in this present paper.

V. Extraction of Beatings in the Presence of Wavelength Jitter

In the mathematical development above, the wavelength scan has not been considered so far since Eq. (13) was used to construct matrix $\mathbf{C}$ (no DFT was performed to deduce the presence of beatings, so the presence of HOMs). Equality between Eq. (12), which holds the information on the wavelength scan, and Eq. (13) is indeed fulfilled provided that cosines are orthogonal to each other ($(\hat{e}_i, \hat{e}_j) = \delta_{ij}$). A legitimate question

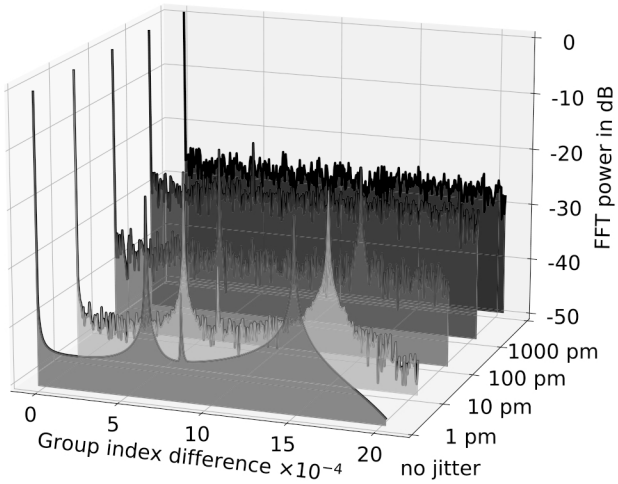

Fig. 8. Standard S^2 analysis. Red curve: DFT obtained with precise values of wavelengths. Three beatings were found (2 major and 1 minor corresponding to $LP_{11}|\ LP_{21}$). Other curves: DFT with wavelengths having random values. Minor peak disappears for a noise greater than 10 pm (green curve), and major peaks are hardly defined when the random noise is greater than 100 pm.

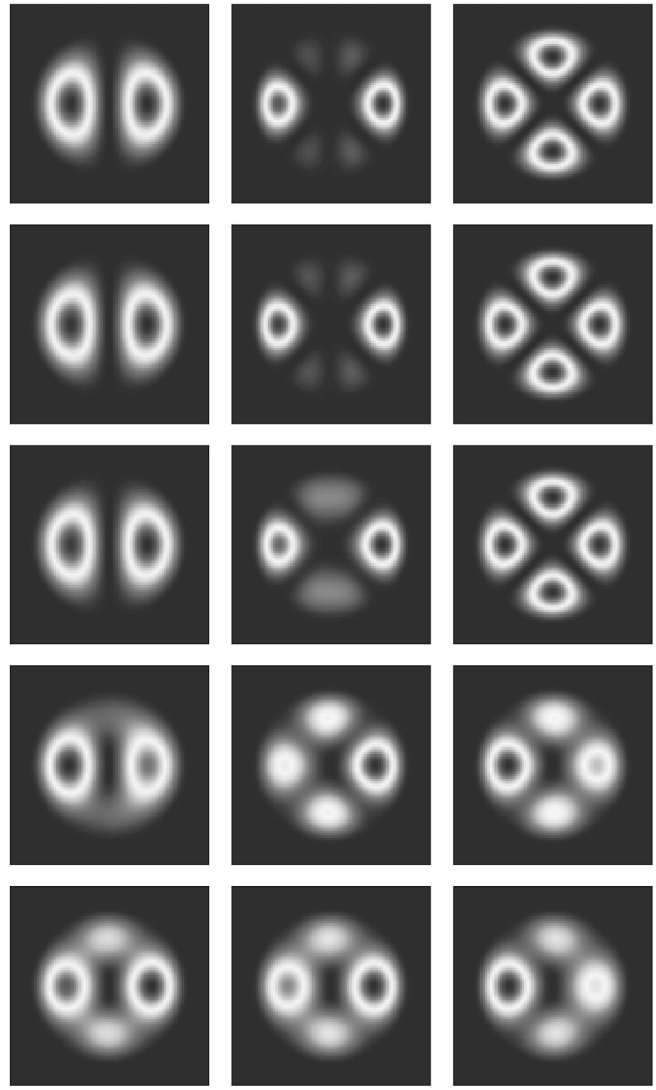

Fig. 9. Standard S^2 analysis. Beating figures are extracted from the S^2 data set using a filter in the Fourier domain. Beatings appear in the order of peaks of Fig. 8 (from left to right). **Top:** no noise. **Bottom:** 1 nm of random noise.

therefore arises concerning the accuracy of the wavelength scan: can we get around the wavelength jitter of the laser source using spatial correlations only?

To do so, we have simulated beatings at the output-end of the 10-m-length 3-mode fiber. Two cases were considered, i.e. constant wavelength step size and non-constant wavelength step (jitter), in order to simulate a laser source with poor scanning precision. LP_{01} is assumed to be the dominant mode with a normalized power of 1.0. A theoretical MPI of -30dB is considered for LP_{11}^E and LP_{21}^E as it allows beatings to be obtained directly without significant error and can be extracted accurately from the standard S^2 analysis [3]. For this example, we did not take into account odd modes since they have the same effective index as the even modes. Other HOMs were not taken into account in this example. Eight hundred and one beating figures (801 wavelengths) are generated between 1030 nm and 1050 nm. To simulate the jitter in wavelength, a random noise was added to each value. We have considered jitter values of 0 pm (ideal scan), 1 pm, 10 pm, 100 pm, and 1000 pm (extreme case) with uniform random noise distribution. Fig. 8 shows the sum of DFTs powers calculated for each pixel (array of 81×81 pixels) as would be done for standard S^2 analysis. The red curve corresponds to the ideal case (no wavelength jitter). The orange, green, blue and black curves correspond respectively to the increasing jitter values. As expected, three peaks can be seen for the expected beatings: two major peaks corresponding to $LP_{01}|\ LP_{11}$ and $LP_{01}|\ LP_{21}$, and one minor for $LP_{11}|\ LP_{21}$. While these peaks are clearly defined in the perfect case, they completely disappear when the jitter is greater than 0.1 nm. For a jitter of 0.01 nm, the minor peak is drowned at the noise level.

The standard S^2 imaging consists in applying a filter in the Fourier domain when peaks appear; each beating is then extracted with its corresponding MPI [3].

MPI is obtained with the formula:

$$\mathrm{MPI} = 10\log_{10}\left(\frac{\int_{A_\infty} I_{\mathrm{HOM}}(x,y)\mathrm{d}A}{\int_{A_\infty} I_1(x,y)\mathrm{d}A}\right) \tag{19}$$

where as per [3], I_{HOM} is the beating pattern obtained by filtering each peak in the Fourier domain, and I_1 is the pattern obtained for the central peak.

Fig. 9 shows the reconstructed beatings as they appear in the DFT in Fig. 8 using standard S^2 analysis. From top to bottom, the jitter noise increases. MPI obtained from this method are summarized in Table II.

Table II shows that the values of MPI are accurately measured when the jitter is low, but for jitter greater or equal to 100 pm, the difference becomes significant. Moreover, beating figures are not correctly reconstructed even for a low jitter of 10 pm as can be seen in Fig. 9, where the second column demonstrates that beating $LP_{11}|\ LP_{21}$ is not correctly displayed. This illustrates

TABLE II
VALUES OF MPI OBTAINED WITH THE STANDARD S^2 METHOD

Jitter (in pm)	MPI for LP_{11}	MPI for LP_{21}
0	-30.02	-30.04
1	-30.02	-30.05
10	-30.08	-30.21
100	-34.35	-37.58
1000	-39.45	-36.99

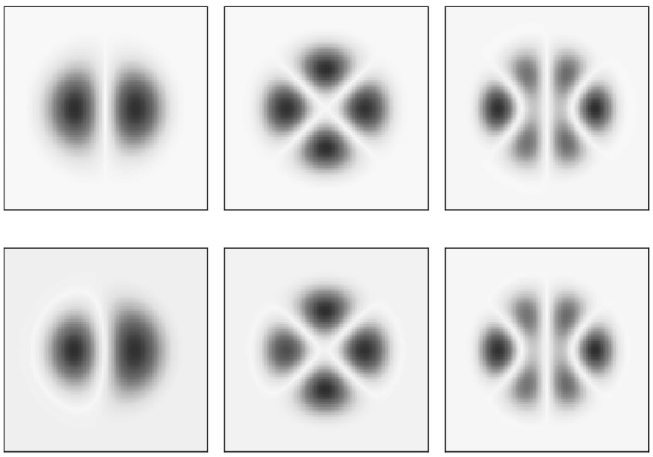

Fig. 10. Three first PCs obtained after diagonalizing variance - covariance matrix. From left to right: the 3 PCs corresponding to $LP_{01}|\,LP_{11}$, $LP_{01}|\,LP_{21}$ and $LP_{11}|\,LP_{21}$) can be recognized. **Top:** no jitter. **Bottom:** jitter of 1 nm.

TABLE III
VALUES OF MPI OBTAINED FROM EIGENVALUES OF VARIANCE - COVARIANCE MATRIX

Jitter (in nm)	MPI for LP_{11}	MPI for LP_{21}
0	-30.00	-30.00
1	-29.99	-30.00
10	-30.05	-29.94
100	-29.83	-30.23
1000	-30.21	-30.21

that the wavelength jitter can be detrimental when performing a standard S^2 imaging.

The procedure described in Section IV is now applied. Fig. 10 shows the three first PCs after diagonalizing the variance-covariance matrix obtained from the 801 generated figures. No DFT is performed at this stage. The top row corresponds to no wavelength jitter, while the bottom raw corresponds to the maximal jitter (1 nm). One can see that major beatings are accurately extracted without the need to use a DFT, even for the high jitter value. The minor PC pattern (right figure) is close to beating $LP_{11}|\,LP_{21}$.

From Eq. (17), MPI are calculated and displayed in Table III. Values obtained with this method are in good accordance with the theoretical ones, even when a jitter as large as 1000 pm was applied.

VI. CONCLUSION

We have demonstrated that beatings can be reconstructed without the use of a DFT by diagonalizing only the variance - covariance matrix $\mathbf{C}$ which can be easily obtained by stacking images of intensities recorded at the output end of the fiber similarly to what is done for a S^2 data acquisition. When the power carried by HOMs is low in comparison to the one carried by the dominant guided mode (usually the LP_{01}), figures of major beatings correspond directly to Principal Components of $\mathbf{X}$, i.e. eigenvectors of matrix $\mathbf{C}$. MPI in each mode are then correctly extracted even in the case of a tunable laser with high wavelength jitter values. In the general case, when no guided mode is mainly excited, MPIs can be theoretically extracted by an optimization method developed to solve general Eq. (15). We believe that this analysis method permits to extend the possibility to perform S^2 analysis even in a wavelength range where no accurate tunable lasers are available (mid-IR or visible range).

APPENDIX

We will assume a fiber supporting 3 guided modes (called $LP_{\,1}$, LP_2, and LP_3 to be more general with respective powers P_1, P_2 and P_3). Three beatings are then expected, which will be called hereafter for sake of clarity: $|B_1\rangle = LP_1|\,LP_2$, $|B_2\rangle = LP_{\,1}|\,LP_3$ (major beatings), and $|B_3\rangle = LP_{\,2}|\,LP_3$, which is the beating supposed to carry less power.

Eq. (13) recalled hereafter:

$$\mathbf{C} = \mathbf{B}\hat{\mathbf{P}}\mathbf{B}^T$$

leads to:

$$\mathbf{C}\,|B_i\rangle = \sum_{k=1}^{M} \lambda_k \,\langle B_k|B_i\rangle\,|B_k\rangle \tag{20}$$

where $\lambda_k = \frac{1}{2}\Pi_k^2$ is a diagonal element of matrix $\hat{\mathbf{P}}$.

We will use the notation $\langle B_i|B_j\rangle = b_{ij}$ to avoid too long equations.

We will assume that 2 beatings are not orthogonal to each other: $|B_1\rangle$ and $|B_3\rangle$ while $|B_2\rangle$ does not couple to $|B_1\rangle$ and $|B_3\rangle$.

From Eq. (14), 3 PCs namely $|V_1\rangle$, $|V_2\rangle$, and $|V_3\rangle$ are expected, which can be decomposed onto the beating basis:

$$\begin{cases} |V_1\rangle = \alpha_{11}\,|B_1\rangle + \alpha_{31}\,|B_3\rangle \\ |V_2\rangle = \alpha_{22}\,|B_2\rangle \\ |V_3\rangle = \alpha_{13}\,|B_1\rangle + \alpha_{33}\,|B_3\rangle \end{cases} \tag{21}$$

Diagonalizing matrix $\mathbf{C}$ implies that PCs (eigenvectors) are orthogonal to each other and also are normalized to unity. In this case, each PC should follow:

$$\begin{cases} \langle V_1|V_1\rangle = \langle V_2|V_2\rangle = \langle V_3|V_3\rangle = 1 \\ \langle V_1|V_2\rangle = \langle V_1|V_3\rangle = \langle V_2|V_3\rangle = 0 \end{cases} \tag{22}$$

Having in mind Eq. (20), one can then calculate each coordinate α_{ji} and each eigenvalue σ_i knowing the power in each mode. Starting for example from the definition of $|V_1\rangle$:

$$\mathbf{C}\,|V_1\rangle = \sigma_1\,|V_1\rangle \tag{23}$$

and using Eqs. (19)–(21), we can obtain the two following equations:

$$\begin{cases} (\alpha_{11}b_{11}+\alpha_{31}b_{13})\alpha_{31} = \frac{\lambda_3}{\lambda_1}(\alpha_{11}b_{13}+\alpha_{31}b_{33})\alpha_{11} \\ A\sigma_1 = \lambda_1(\alpha_{11}b_{11}+\alpha_{31}b_{13})\alpha_{33} - \lambda_3(\alpha_{11}b_{13}+\alpha_{31}b_{33})\alpha_{13} \end{cases}$$

where $A = \alpha_{11}\alpha_{33} - \alpha_{31}\alpha_{13}$.

The first equation of this system leads to:

$$b_{13}\beta^2 + (b_{11} - b_{33}\epsilon)\beta - b_{13}\epsilon = 0 \tag{24}$$

where $\beta = \alpha_{31}/\alpha_{11}$ and $\epsilon = \lambda_3/\lambda_1 = P_3/P_1 \ll 1$, if we assume that LP_1 is mainly excited.

Thus one can obtain for PC $|V_1\rangle$:

$$\beta = \frac{-b_{11} + b_{33}\epsilon + \sqrt{(b_{11}-\epsilon b_{33})^2 + 4b_{13}^2\epsilon}}{2b_{13}}$$

From $\langle V_1|V_1\rangle = 1$, we obtain expression of α_{11}:

$$\alpha_{11} = \frac{1}{\sqrt{b_{11} + 2b_{13}\beta + b_{33}\beta^2}}$$

A Taylor expansion assuming $\epsilon \ll 1$ gives:

$$\alpha_{11} = \frac{1}{\sqrt{b_{11}}}\left(1 - \frac{b_{13}^2}{b_{11}^2}\epsilon + \frac{5b_{13}^4 - 3b_{11}b_{33}b_{13}^2}{2b_{11}^4}\epsilon^2\right) + o(\epsilon^3) \tag{25}$$

From definition of β, α_{31} can be determined:

$$\alpha_{31} = \frac{1}{\sqrt{b_{11}}}\left(\frac{b_{13}}{b_{11}}\epsilon - \frac{b_{13}}{b_{11}^3}(2b_{13}^2 - b_{11}b_{33})\epsilon^2\right) + o(\epsilon^3) \tag{26}$$

From Eq. (25), one can deduce that at low power in HOMs, the major eigenvector $|V_1\rangle$ is approximately proportional to $|B_1\rangle$:

$$|V_1\rangle \approx \frac{1}{\sqrt{b_{11}}}|B_1\rangle$$

Of course, Eqs. (20) and (21) tell us that the second major PC, orthogonal to the other ones, is given by:

$$|V_2\rangle = \frac{1}{\sqrt{b_{22}}}|B_2\rangle$$

This development corresponds to the numerical results shown in Section IV-A.

Similarly, $\mathbf{C}|V_3\rangle = \sigma_3|V_3\rangle$ gives a set of similar equations. Assuming that $\gamma = \alpha_{33}/\alpha_{13}$, we obtain:

$$\gamma = \frac{-b_{11} + b_{33}\epsilon - \sqrt{(b_{11}-\epsilon b_{33})^2 + 4b_{13}^2\epsilon}}{2b_{13}}$$

$\langle V_3|V_3\rangle = 1$ leads to:

$$\alpha_{13} = \frac{1}{\sqrt{b_{11} + 2b_{13}\gamma + b_{33}\gamma^2}}$$

A Taylor expansion yields:

$$\alpha_{13} = \frac{b_{13}}{\sqrt{b_{11}}\sqrt{b_{11}b_{33} - b_{13}^2}}\left(1 + \frac{b_{11}b_{33} - b_{13}^2}{b_{11}^2}\epsilon\right) + o(\epsilon^2) \tag{27}$$

and

$$\alpha_{33} = \frac{\sqrt{b_{11}}}{\sqrt{b_{11}b_{33} - b_{13}^2}}\left(-1 + \frac{b_{13}^2}{2b_{11}^4}(b_{11}b_{33} - b_{13}^2)\epsilon^2\right) + o(\epsilon^3) \tag{28}$$

This result implies that the minor PCs are not beating figures, but a combination of them, since α_{13} and α_{33} have similar orders of magnitude, even at low MPIs, which is coherent with the results of Section IV-A. Moreover, when ϵ is not too high, coordinates α_{13} and α_{33} are approximately constant to the order of ϵ. This is coherent with the fact that minor PC patterns do not change significantly when power P in HOMs is not too high.

Using Eq. (20), and after some calculations, we can get for the eigenvalues σ_1, σ_2, and σ_3:

$$\begin{cases} \sigma_1 = \lambda_1(b_{11} - b_{13}\epsilon/\gamma) \\ \sigma_2 = \lambda_2 b_{22} \\ \sigma_3 = \lambda_1(b_{33}\epsilon - b_{11}\beta) \end{cases}$$

A Taylor expansion of σ_1 and σ_3 gives:

$$\begin{cases} \sigma_1 \approx \lambda_1 b_{11}(1 + \frac{b_{13}^2}{b_{11}}\epsilon) + o(\epsilon^2) \\ \sigma_3 \approx \lambda_3 b_{33}(1 - \frac{b_{13}^2}{b_{33}b_{11}}) + o(\epsilon^2) \end{cases}$$

REFERENCES

[1] D. M. Nguyen *et al.*, "Modal decomposition technique for multimode fibers," *Appl. Opt.*, vol. 51, no. 4, pp. 450–456, Feb. 2012.

[2] J. W. Nicholson, A. D. Yablon, S. Ramachandran, and S. Ghalmi, "Spatially and spectrally resolved imaging of modal content in large-mode-area fibers," *Opt. Exp.*, vol. 16, no. 10, pp. 7233–7243, May 2008.

[3] J. W. Nicholson, A. D. Yablon, J. M. Fini, and M. D. Mermelstein, "Measuring the modal content of large-mode-area fibers," *IEEE J. Sel. Top. Quantum Electron.*, vol. 15, no. 1, pp. 61–70, Jan. 2009.

[4] C. Jauregui, T. Eidam, J. Limpert, and A. Tünnermann, "Impact of modal interference on the beam quality of high-power fiber amplifiers," *Opt. Exp.*, vol. 19, no. 4, pp. 3258–3271, Feb. 2011.

[5] T. Mizuno and Y. Miyamoto, "High-capacity dense space division multiplexing transmission," *Opt. Fiber Technol.*, vol. 35, pp. 108–117, 2017.

[6] B. Sévigny *et al.*, "Advanced s^2 imaging: Application of multivariate statistical analysis to spatially and spectrally resolved datasets," *IEEE J. LightW. Technol.*, vol. 32, no. 23, pp. 4606–4612, Dec. 2014.